



Photocatalytic activity and removal of organic dyes using sulfated zirconia Prepared by a new method

Talaat Elerian, Shady M. El Dafrawy, Shawky Hassan

Chemistry Department, Faculty of Science, Mansoura University



CrossMark

Abstract

Sulfated zirconia has been studied widely in recent years, particularly for its potential applications as solid catalysts in acid-catalyzed reactions. In addition, it has oxidizing properties that may play a role in synthesizing organic compounds. This paper introduces a series of $\text{SO}_4^{2-}/\text{ZrO}_2$ catalysts precipitated at different sulfuric acid concentrations (1–3 N) using a sol-gel method. The prepared catalysts were calcined at 300°C, 400°C and 500°C. In particular, surface acidity was measured using the *n*-butylamine method and by pyridine adsorption. A sulfated zirconia tetragonal phase was prepared in an acidic medium 1N H_2SO_4 . An amorphous to crystalline phase transformation occurred when the calcination temperature was increased. The incorporation of SO_4^{2-} in ZrO_2 increased the surface acidity of the catalysts. Moreover, acidity increased with increasing calcination temperature from 300°C to 500°C and then decreased. Hydrated zirconia was precipitated in an acidic medium followed by calcination to produce solid materials with useful properties that favor their application in photocatalysis by studying degradation of MB and MO dyes in water.

Keywords: Sol-gel method, SZ, Calcination temperature, Acidity, Photocatalysis

1. Introduction

Zirconium oxide and zirconium compounds are increasingly recognized as valuable catalytic materials. In particular, zirconium oxide (zirconia) is an important support material for catalysis, having both acidic and basic properties [1]. Zirconia has an additional advantage in that the natures of the active sites are known and can be defined by the generated Brønsted and Lewis acid sites. Many methods have been explored to obtain superfine ZrO_2 powders (e.g., hydrothermal process, vapor phases hydrolysis, gas condensation, sol-gel process, and combustion methods [2-3]).

Sulfated zirconia has attracted considerable interest and has been studied intensively in the last 20 years [4]. Currently, it is recognized as very strong acid and possesses all the advantages of heterogeneous catalysts (e.g., easy separation, recovery, and reutilization). This material exhibits high catalytic activity in many industrially important reactions [5].

SO_4^{2-} -doped zirconia samples have attracted considerable interest because of their strong acid characteristics and their consequent potential as solid acid catalysts for selective hydrocarbon isomerization and several other acid-promoted reactions. This material is classically synthesized by

the precipitation of zirconium hydroxide from the hydrolysis of ZrOCl_2 aqueous salt solutions [6-8]

The sol-gel template method is popular because of its distinctive advantages (e.g., high purity, homogeneous multicomponent nanoparticles, and the easy chemical doping of the prepared materials; [9-10]). This method typically entails the hydrolysis of a solution to obtain colloidal particles (sol), and a gel then forms. The latter point of particular importance for the surface area of zirconia is usually relatively low at 20–50 m^2/g , and different routes to obtaining high surface area zirconia have been reported [11-12]. Several studies have confirmed that the acidity of sulfated zirconia is weaker than the acidity of pure sulfuric acid [13-14].

This study provides evidence for the role of the sol-gel preparative variables and surface features of sulfated zirconia catalysts as well as the effect of the starting salts on the sol-gel method. In addition, this study examined the correlation between the catalytic properties of sulfated zirconia samples resulting from the calculations of a sulfated zirconium hydroxide between 300°C and 500°C and their acidic properties.

2. MATERIALS AND METHODS

Zirconium hydroxide was prepared by a sol-gel method from zirconium nitrate salt was dissolved in ethanol [15] and precipitated by the dropwise

*Corresponding author e-mail: shomirage@yahoo.com (Shady M. El Dafrawy).

Receive Date: 18 July 2022, Revise Date: 29 July 2022, Accept Date: 16 August 2022

DOI: 10.21608/EJCHEM.2022.150914.6538

©2022 National Information and Documentation Center (NIDOC)

addition of H₂SO₄ (Analar) with vigorous stirring. Subsequently, these gels were dried at 90°C for 3 hrs at rotary evaporator to obtain SZ powder, followed by calcination at 300°C, 400°C, and 500°C for 3 h. In the designation of these samples, the letters S and Z denote SO₄²⁻ and ZrO₂, respectively. The roman numbers I, II, and III refer to the calcination temperatures of 300°C, 400°C, and 500°C, respectively, while the Arabic numbers 1, 2, and 3 represent the SO₄ concentration. For example, the designation 1SZI indicates the sample precipitated by 1N H₂SO₄ and calcined at 300°C.

2.1 Characterization

XRD patterns was evaluated using PW 150 (Philips) using Ni-filtered Cu K α radiation in the 2 θ range of 10°-80° to identify the formation of SZ nanoparticles phases and crystal size as a non-destructive method [16] using the following equation:

$$\% \text{ Tetragonal} = \left[\frac{IT(2\theta = 30.15)}{IT(2\theta = 30.15) + \left(\frac{IM(2\theta = 28.16) + IM(2\theta = 31.44)}{2} \right)} \right] \times 100$$

The crystallite size was calculated to be 30.15 nm from the reflection of the tetragonal zirconia phase at 2 h using the Scherer relationship

$$D = \frac{k\lambda}{\beta \cos \theta}$$

Where k , λ , β , and θ are the crystallite shape constant (≈ 1), radiation wavelength (Å), line breadth (radians), and Bragg angle, respectively.

The total acidity of all the catalysts was determined using the *n*-butyl amine titration method [17] using an Orion 420 digital A model with a double junction electrode. In this method, 0.2 g of catalyst was heated under a vacuum, and 10 mL of acetonitrile was added. The suspension was titrated with 0.01 N *n*-butyl amines in acetonitrile after 2-h agitation. The addition continued until no further change in mV was recorded. The wavelength and absorbance of the prepared photocatalysts were measured using an ultraviolet–visible (UV–Vis) reflectance spectrophotometer to determine the bandgap from the Kubelka–Munk equation. The particle sizes of ZrO₂ and SO₄²⁻/ZrO₂ particles were determined by scanning electron microscopy (SEM; JSM-5900 LV) at an accelerating voltage of 20 kV. The Fourier-transform infrared (FTIR) spectroscopy of the adsorbed basic molecules, particularly pyridine, is used to examine the surface acidity (both Lewis and Brønsted types) of the catalysts. The FTIR spectra of pyridine adsorbed on the acid sites of the catalysts exhibited bands characteristic of Lewis and Brønsted acid sites. The percentage of Lewis–Brønsted acid sites can be calculated using the integrated areas or the relative intensity of the characteristic bands of pyridine adsorbed on Lewis and Brønsted acid sites. Photocatalytic activities of the SO₄²⁻/ZrO₂ nanoparticles were estimated by

studying the degradation of MB and MO dyes in water using UV–Vis light irradiation at 20°C by external lamp (Halogen Mercury lamp, 400 W UV/Vis lamps).

3. RESULTS

3.1 XRD

This study investigated the main features of zirconia samples precipitated by sulfuric acid. The beneficial effect of the SO₄²⁻ group on the surface and tetragonal phase of zirconia were examined by XRD. The phase composition and crystallite sizes were also determined for all the precursors and calcined samples, as described in the characterization section. Figures 1 and 2 shows the effects of the sulfuric acid concentration and calcination temperature on the crystal size and percentage of the tetragonal phase. The tetragonal phase increased with increasing SO₄²⁻ concentration to 2 N and then decreased.

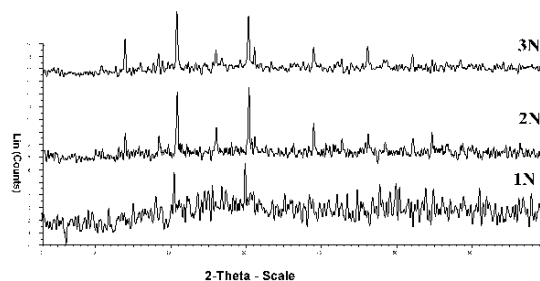


Fig. 1: X-ray diffraction patterns of the different SZI concentration, 1SZ I, 2SZ I and 3SZ I

A phase change from amorphous to crystalline (tetragonal and monoclinic) occurred as the calcination temperature increased as shown in Fig 2.

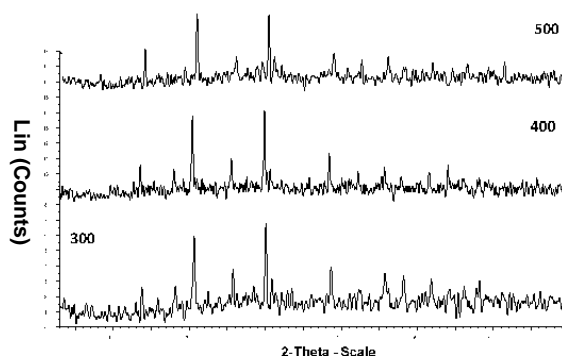


Fig. 2: X-ray diffraction patterns of 2SZ samples calcined at (a) 300°C, (b) 400°C, (c) 500°C

3.2. UV–Vis absorption spectroscopy analysis

Figures 3, 4 present the band gap variation. The absorbance was analyzed using the Kubelka–Munk equation to obtain the $(\alpha h\nu)^2$ values. An extrapolation of the linear region of $(\alpha h\nu)^2$ vs. $h\nu$ for the SO₄²⁻/ZrO₂ films indicated that the band gap of the nanocomposites decreased slightly with an

increasing ZrO_2 quantity in $\text{SO}_4^{2-}/\text{ZrO}_2$. The ZrO_2 bandgap energy was determined as 3.25 eV. The bandgap of the $\text{ZrO}_2/\text{SO}_4^{2-}$ nanocomposite films ranged from 3.95 to 3.2 eV. The bandgap energy caused a redshift in the absorption peak with increasing ZrO_2 content. This decrease in bandgap energy may be due to the formation of a charge-transfer complex from the trap levels between the HOMO and LUMO energy states of SO_4^{2-} , which promotes lower energy transitions leading to the observed change in the bandgap.

The E_g values of ZrO_2 and $\text{SO}_4^{2-}/\text{ZrO}_2$ were 3.27 and 3.55 eV, respectively. The band gaps of the samples containing SO_4^{2-} were 3.10–3.16 eV, which were smaller than those of pure oxides.

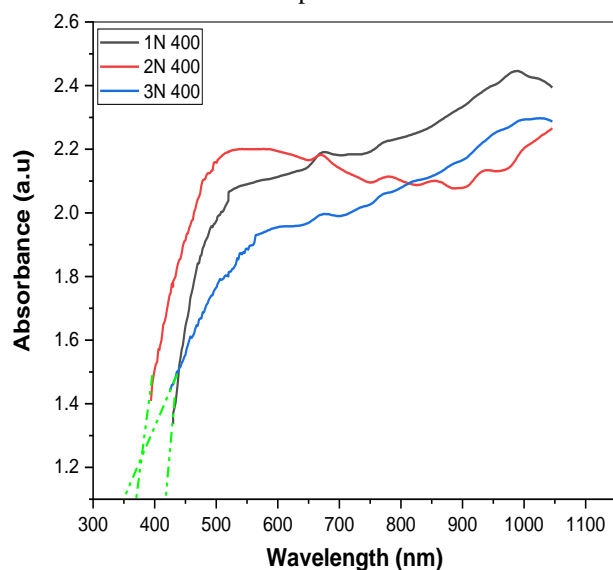


Fig 3 UV-Vis absorbance of the different SZI concentration, 1SZ I, 2SZ I and 3SZI

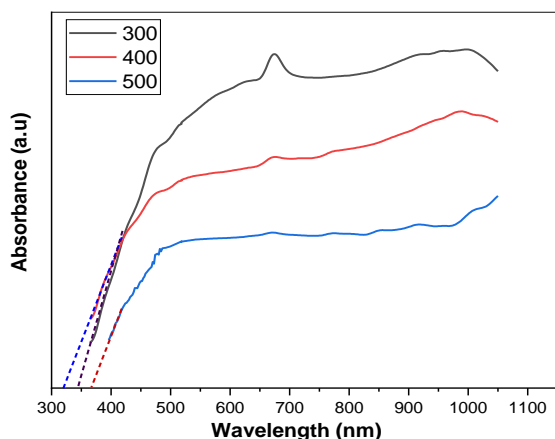


Fig 4 UV-Vis absorbance of 2SZ samples calcined at (a) 300°C, (b) 400°C and (c) 500°C

3.3. SEM analysis

Figure 5 and 6 present SEM images of selected ZrO_2 and $\text{SO}_4^{2-}/\text{ZrO}_2$ photocatalysts with various SO_4^{2-} contents (1N, 2N, and 3N) in which agglomeration can be observed for all the samples to

some extent. This particle aggregation may lead to the difference observed in the particle size obtained through the XRD and SEM analyses for ZrO_2 and $\text{SO}_4^{2-}/\text{ZrO}_2$. In addition, SEM showed that the hexagonal phase increased with increasing SO_4^{2-} content. Small crystals with various phases were interwoven, producing strongly bound nanoclusters.

SEM was also used to confirm the distribution and size of ZrO_2 in crystal structure. ZrO_2 appeared as white spots and its particles were well spread. This showed that good adhesion between the surface of the ZrO_2 nanoparticles and ZrO_2 was achieved by modifying the surface of the ZrO_2 nanoparticles.

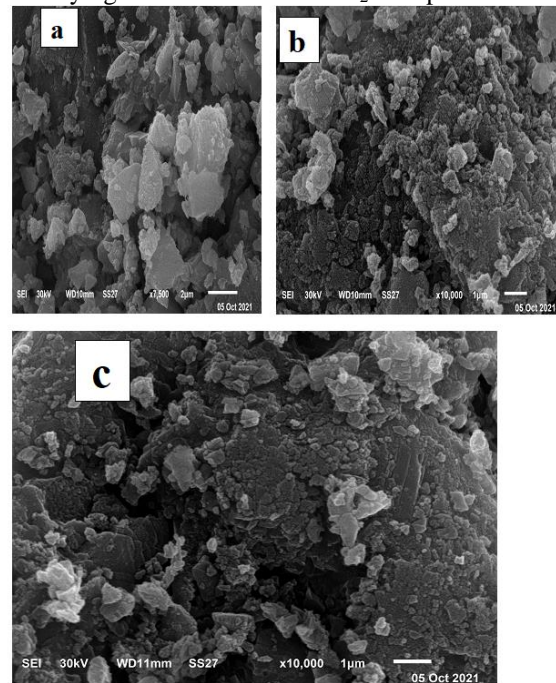


Fig 5 SEM image of the different SZI concentration, 1SZ I, 2SZ I and 3SZ I

3.4. Surface acidity

The surface acidity of the investigated catalysts was determined by a nonaqueous titration of *n*-butyl amine ($\text{pK}_a = 10.73$), which is a basic molecule suitable for titrating the medium and strong acid sites on the surface of the investigated catalysts [18]. The buffer behavior was more apparent as the acid sites of the solid become neutralized. Thus, the trend of the titration curve is asymptotic, leading to a characteristic value on the potential (in mV) axis, which in turn is related to the *n*-butyl amine volume per gram needed to neutralize surface acidity [15]. The magnitude of the change for the electrode potential in this method is related to the surface acidity of the catalyst [19]. Table 1 shows the volume of *n*-butyl amine per gram required to neutralize the surface acidity of some prepared catalysts and the total number of acid sites per gram. This technique was conducted by measuring the electrode potential (in mV) and pH as a function of the *n*-butyl amine concentration added (in mmole *n*-butyl amine per

gram catalyst). The total number of acid sites per gram of the catalysts was calculated using the following equation:

Total number of acid sites per gram = (mL equiv/g) \times $N \times 1,000$ (where N is the Avogadro's number).

Table 1. Acidity parameters of the investigated catalysts:

Calcination ($^{\circ}\text{C}$)	Concentration (N)	Total no. of acid sites
300	1	1.44×10^{23}
	2	3.90×10^{23}
	3	1.00×10^{24}
400	1	1.20×10^{23}
	2	5.78×10^{23}
	3	1.05×10^{24}
500	1	5.48×10^{23}
	2	8.60×10^{23}
	3	9.33×10^{23}

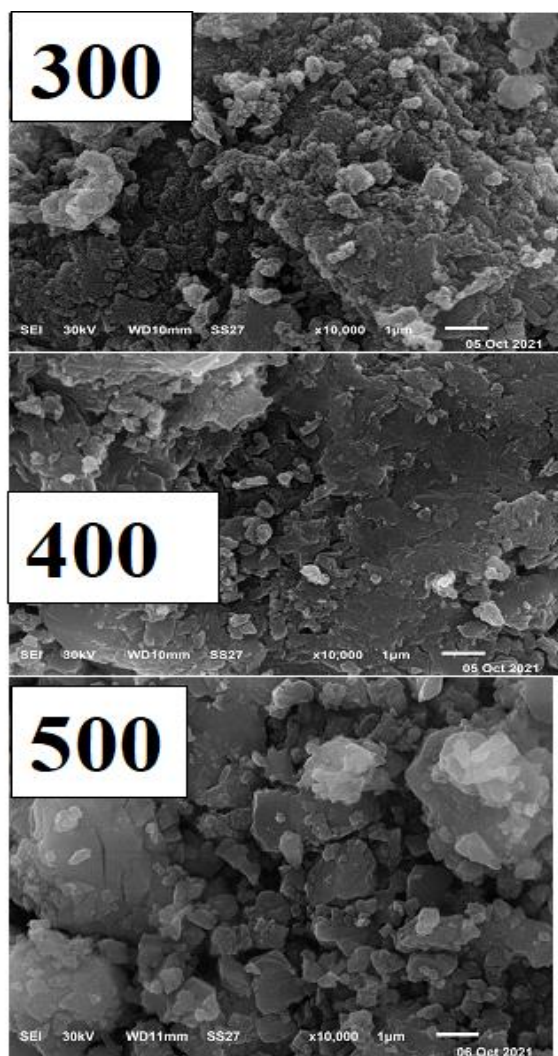


Fig 6 SEM images for 2SZ samples calcined at (a) 300 $^{\circ}\text{C}$, (b) 400 $^{\circ}\text{C}$, (c) 500 $^{\circ}\text{C}$

FTIR spectroscopy was conducted at room temperature [20]. A 0.05-g sample was degassed for ~ 2 h at 250 $^{\circ}\text{C}$ to reduce the amount of adsorbed molecular water. The samples were maintained in contact with pyridine vapor at room temperature for 1 month before mixing 0.05 g of the sample with 0.1 g of potassium bromide to produce a 30-mm diameter self-supporting disk. The FTIR spectra of the 0.05 g of the samples were recorded at room temperature in the 1,700–1,400 cm^{-1} region.

The sulfated zirconia samples contain a mixture of Brønsted and Lewis acid sites, calculated from pyridine adsorption (Figure 7). Moreover, the Brønsted and Lewis acidity were quantified from the integrated areas of the absorbance bands at 1,541 and 1,446 cm^{-1} , respectively. The number of Brønsted and Lewis acid sites was calculated. The advantages of this technique are as follows. The Brønsted (B) and Lewis (L) acid sites can be distinguished because the IR spectra of adsorbed pyridine show characteristic differences. In situ pretreatments can be given to the catalyst, and the acid strength distribution of sites can be investigated by monitoring the pyridine thermodesorption [21]. The acid types on the surface of a solid acid can be differentiated because the spectrum of pyridine coordinately bonded to the surface is very different from that of the pyridinium ion [22]. The shift in the band wavenumber to higher values suggests that the strength of the acid sites increases based on the frequency shift of one of the bands of coordinately bonded pyridine compared to that in the liquid phase. In contrast, the shift to a lower wavenumber suggests that the strength of the acid sites decreases.

3.5. Photocatalytic activity

The photocatalytic activity of the prepared ZrO_2 and $\text{SO}_4^{2-}/\text{ZrO}_2$ catalysts for MB and MO degradation under irradiation with UV–Vis light was evaluated. First, a dry clean bottle containing 50 mL of a dye solution (10 ppm) and a 0.1 mg/L catalyst were stirred for 30 min in the dark. Subsequently, the bottle was irradiated with UV–Vis light for a certain time. A 1 mL aliquot was taken, diluted 10 times, and centrifuged for 15 min to allow the catalyst to settle. The dye concentration was measured using a UV–Vis spectrophotometer at a certain wavelength according to the λ_{max} of each dye (666 nm for MB and 464 nm for MO). The percentage removal was evaluated using the following equation:

$$\% \text{ removal} = \frac{C_0 - C_t}{C_0} * 100$$

C_0 is the initial concentration of dye (in milligrams per liter) and C_t is the concentration of dye (in milligrams per liter) at time t (in minutes).

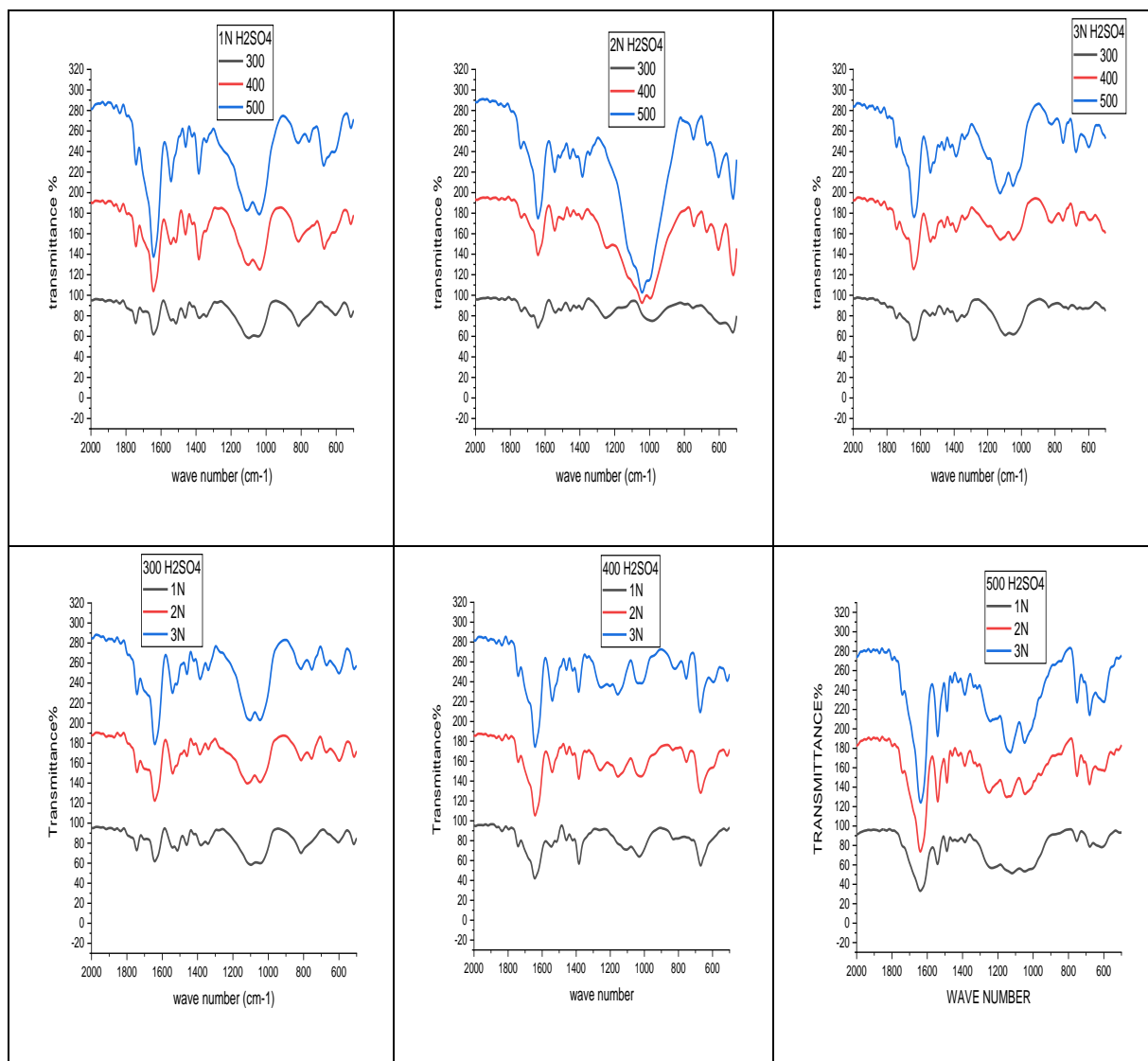


Fig 7 : FT-IR spectra of pyridine adsorbed of the different SZ samples

The effect of the SO_4^{2-} concentration on the MB degradation was examined. Doping is an effective method of improving the activity of a wide band gap photocatalyst (e.g., ZrO_2). The results summarized in figs 8, 9 shows that ZrO_2 exhibited lower photocatalytic activity and a higher number of acid sites than those of $\text{SO}_4^{2-}/\text{ZrO}_2$. For the MB cationic dye, the low ZrO_2 photocatalytic activity may be due to rapid electron-hole recombination and participation of a small part of these electrons and holes in the photocatalytic reaction.

Among the $\text{SO}_4^{2-}/\text{ZrO}_2$ catalysts, $\text{ZrO}_2/5\text{SO}_4^{2-}$ had the optimal doping level, leading to the maximum photocatalyst activity, which stems from the influence of SO_4^{2-} in decreasing the recombination rate and creating a new ZrO_2 energy level. The photocatalytic activity decreased with increasing SO_4^{2-} content beyond 2N (Fig 8). This was attributed to the high

SO_4^{2-} content increasing the electron-hole recombination rate.

The effect of the calcination temperature on MB degradation was examined. SEM, XRD, and UV-Vis spectroscopy showed that the calcination temperature has a significant effect on the bandgap and structure of the catalysts, eventually affecting the photocatalytic performance. The photocatalytic activity of $\text{ZrO}_2/\text{SO}_4^{2-}$ for the photodegradation of the MB cationic dye at calcination temperatures of 300°C, 400°C, and 500°C is presented in Figure 9. The $\text{SO}_4^{2-}/\text{ZrO}_2$ nanocomposite exhibited the best photocatalyst activity at a calcination temperature of 400°C, as confirmed by SEM and XRD.

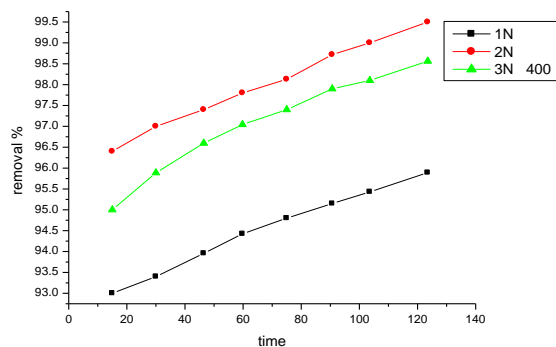


Fig 8 Photocatalytic degradation curve of a the different SZ concentration, 1SZ, 2SZ and 3SZ calcined at 300

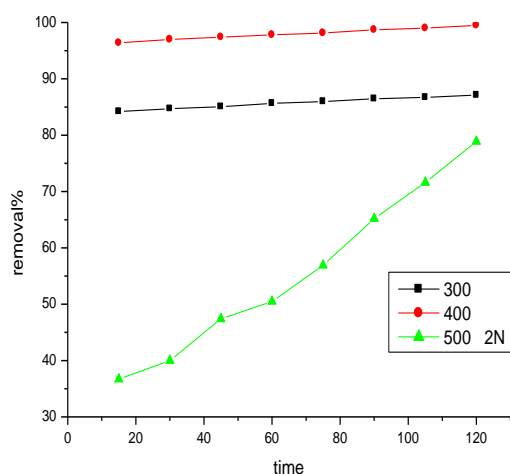


Fig 9 Photocatalytic degradation curve of 2SZ samples calcined at (a) 300°C, (b) 400°C, (c) 500°C.

4. DISCUSSION

XRD highlighted the importance of the SO_4^{2-} introduction step in the crystal phase development of sulfated zirconia. This feature could have been expected based on the already reported role of the SO_4^{2-} in stabilizing the tetragonal polymorph [13] and delaying the growth of zirconia crystallites [14]. The tetragonal phase increased with increasing the SO_4^{2-} concentration to 2 N and then decreased at higher concentrations. All the sample precursors calcined below 300°C were amorphous. In contrast, the samples calcined at temperatures 400°C behaved differently and began to crystallize. The monoclinic (28° and 31° 2θ) and tetragonal (30° 2θ) phases appeared as shown in XRD, depending on the SO_4^{2-} content, accompanied by crystallite growth and instability of the tetragonal phase, indicating the

sintering of zirconia particles due to the elimination of H_2O and SO_3 .

XRD showed that the tetragonal phase increased with increasing sulfuric acid concentration up to 2 N, followed by a decrease.

The potentiometric titration curves were obtained to calculate the total number of acid sites. The number of acid sites increased with increasing sulfuric acid concentration due to the number of SO_4^{2-} groups bonded to the zirconia surface. Therefore, an SO_4^{2-} -Zr interaction could be responsible for the acidity of the catalysts. The samples calcined at 400°C produced higher surface acidity and was the optimal calcination temperature where the total surface acidity was maximum. A further increase in calcination temperature to 500°C led to a significant decrease in total acidity. The loss of surface acidity at higher calcination temperatures (500°C) for all samples may be due to the evolution of SO_3 that decomposes from the SO_4^{2-} group bonded to the zirconia surface.

The pyridine adsorption technique enables an evaluation of the surface and the bulk acidity because of the high absorptivity of the SO_4^{2-} acid catalyst to polar molecules as pyridine [23-24,16]. In addition to the reaction with the surface protons, pyridine also penetrates and reacts with the bulk acid sites of SZ. The integrated area of the pyridine band is a measure of the number of Brønsted and Lewis acid sites. The intensity of the Brønsted band pyridine ($1,541\text{ cm}^{-1}$) and that for the Lewis band ($1,446\text{ cm}^{-1}$) changed with the SO_4^{2-} concentration on zirconia and the calcination temperature.

SO_4^{2-} groups generate strong Lewis and Brønsted acidity when adsorbed on the surface of SZ. SO_4^{2-} species are Lewis acid sites that, by attracting electrons, generate Lewis acid centers on the oxide surface. These Lewis acid sites increased the Brønsted acid strength of the surface of hydroxyl groups present on the surface. Moreover, the chemical state of the SO_4^{2-} groups sometimes determined the acidity of the oxide surface [25]. These results suggest that the distribution and the number of SO_4^{2-} groups on the zirconia surface is a maximum responsible for the higher acidity reaching a maximum at 400°C. At calcination temperatures higher than 500°C, the SO_4^{2-} group on the zirconium oxide surface decomposes. Hence, the surface acidity decreases.

5. CONCLUSION

Based on the aforementioned findings, the following are the main points that could be summarized. The tetragonal phase in the zirconia samples increased with increasing SO_4^{2-} concentration to 2 N and then decreased at higher concentrations. By contrast, the sample calcined at 300°C–500°C was amorphous or poorly crystalline, while an increase in calcination temperature resulted in tetragonal and monoclinic phases. The SO_4^{2-} -Zr interaction and the

calcination temperature could be responsible for the acidity. The acidity increased with increasing H₂SO₄ concentration due to the increase in SO₄²⁻ concentration. The calcination temperature, up to 400°C, increased the acidity, but the acidity decreased at calcination temperatures higher than 500°C because the SO₄ decomposed to SO_x. Photodegradation of MB and MO dyes in water by SZ was the best at calcination 400°C and 2N concentration of H₂SO₄.

REFERENCES

- 1) Chuah G. K., S. Jaenicke, S. A. Cheong, and K. S. Chan., The influence of preparation conditions on the surface area of zirconia J. Appl. Catal. A: Gen. 1996, 145, 267.
- 2) Ray, J. C., C. R. Saha, and P. Pramanik., Stabilized nanoparticles of metastable ZrO₂ with Cr³⁺/Cr⁴⁺ cations: Preparation from a polymer precursor and the study of the thermal and structural properties J. Eur. Ceram. Soc. 2002, 22, 851.
- 3) Luo T. Y., T. X. Liang, and C. S. Lui., Effect of the support porosity on the thiophene and dibenzothiophene hydrodesulphurization reactions. Al₂O₃-TiO₂ mixed oxide support J. Univ. Sci. Technol. Beijing 2005, 12,365.
- 4) Yamaguchi T., Recent progress in solid super acid J. Appl. Catal. 1990, 61: 1.
- 5) Zhao J., Y. Yue, W. Hua, H. He, and Z. Gao., Catalytic activities and properties of sulfated zirconia supported on mesostructured γ -Al₂O₃ J. Appl. Catal A: Gen. 2008, 336, 133.
- 6) Morterra C., G. Cerrato, F. Pinna, M. Signoretto, and G. Strukul., On the acid-catalyzed isomerization of light paraffin's over a zro2/so4 system: The effect of hydration J. Catal 1994, 149, 81.
- 7) Melada S., S. A. Ardizzzone, C. L. Bianchi., Sulfated zirconia by sol-gel route. The effects of the preparative variables J. Micropor. Mesopor. Mater. 2004, 73, 203.
- 8) Li C., T. Liang, and T. Uo., Preparation of ZrO₂ nanoparticles by the hydrolysis of ZrOCl₂ solution in the reverse micelles. J. Univ. Sci. Technol. Beijing 2006, 13, 355
- 9) Yang Z., Y. Huang, B. Dong, and H. L. Li., Template induced sol-gel synthesis of highly ordered LaNiO₃ nanowires J. Solid State Chem. 2005, 178, 1157.
- 10) Yang Z., Y. Huang, B. Dong, and H. L. Li., Controlled synthesis of highly ordered LaFeO₃ nanowires using a citrate-based sol-gel route J. Mater. Res. Bull. 2006, 41, 247.
- 11) Ozawa M. and M. Kimura., Preparation of zirconia powder by the pyrolysis of active carbon J. Mater. Sci. Lett. 1990, 9, 446.
- 12) Ciesla U., S. Schacht, G. D. Stucky, K. K. Unger, and F. Schuth, Formation of a porous zirconium oxo phosphate with a high surface area by a surfactant-assisted synthesis angew. Chem. Int. Ed. Engl. 1996, 35, 541.
- 13) Babou F., B. Bigot, G. Coudurier, P. Sautet, and J. C. Vedrine., Sulfated zirconia for n-butane isomerization experimental and theoretical approaches J. Stud. Surf. Sci. Catal. 1994, 90, 519.
- 14) Babou F., G. Coudurier, and J. C. Veâdrine., Hydrocarbon deposits formed during n-butane isomerization on sulfated zirconia J. Top Catal. 1995, 152,341.
- 15) Dominguez J. M., J. L. Hernandez, and G. Sandoval., Surface and catalytic properties of Al₂O₃-ZrO₂ solid solutions prepared by sol-gel methods J. Appl. Catal. 2000, 197, 119.
- 16) Devassy B. M., F. Lefebvre, W. Bohringes, J. Fletcher, and S. B. Halligudi., Synthesis of linear alkyl benzenes over zirconia-supported 12-molybdophosphoric acid catalysts J. Mol. Catal. A: Chem. 2005, 236, 162.
- 17) Shady M. EL-Dafrawy, Mahmoud Tarek, Salem Samra and Shawky M. Hassan, Synthesis, photocatalytic and antidiabetic properties of ZnO/PVA nanoparticles, 2021, 11, 11404
- 18) Pecchi G. and R. Cid., Potentiometric method for determining the number and relative strength of acid sites in colored catalysts J. Appl. Catal. 1985, 14, 15.
- 19) Barrett E. P., L. G. Joyneand, and P. Halenda., Pore distributions from desorption isotherms J. Am. Chem. Soc. 1951, 73, 373.
- 20) Tanabe K., Tokyo, Solid Acids and Bases Their Catalytic Properties 1970, 1
- 21) Parry E. P., Catalytic properties of sulfated and non-sulfated ZrO₂-SiO₂ J. Catal. 1963, 2,371.
- 22) De Castro C., J. Primo, and A. Corma., The Friedel-Crafts acylation of anisole (AN) with acetic anhydride (AA) in liquid phase catalysed by bulk and silica-supported heteropoly acids (HPA) J. Mol. Catal. A: Chem. 1998, 134, 215.
- 23) Sun Y., L. Zhu, H. Lu, R. Wang, S. Lin, D. Jiang, and F. S. Xiao., Meso structured sulfated zirconia with high catalytic activity in n-butane isomerization J. Appl. Catal. 2002, 237, 21.
- 24) Das D., H. K. Mishra, A. K. Dalai, and K. M. Parida., Synthesis, characterization and activity study of SO₄²⁻/Ce_xZr_{1-x}O₂ solid superacid catalyst J. Appl. Catal. A: Gen. 2003, 271, 243.
- 25) Fares T. Elshorifi, Shady M. El Dafrawy, Awad I. Ahmed, Fe/Co-MOF nanocatalysts: Greener chemistry approach for the removal of toxic metals and catalytic applications, 2022, 7, 23421